Compressibility of elastomer matrix-hollow thermoplastic microspheres composites under low hydrostatic pressure

Ruelle Baptiste, Pierre Rublon, Michel Coret, Erwan Verron

Compressibility of elastomer matrix–hollow thermoplastic microspheres composites under low hydrostatic pressure

Ruelle B.[1,2], Rublon P.[2], Coret M.[1], and Verron E. [*,1]

[1]Nantes Universit, École Centrale Nantes, CNRS, GeM, UMR 6183, F-44300 Nantes, France

[2]Naval Group, Technocampus Ocean, rue de lHalbranne, 44340, Bouguenais, France

December 20, 2024

Abstract

This paper investigates the pressure-volume response of elastomer matrix composites filled with hollow thermoplastic microspheres and subjected to low hydrostatic pressure. The hysteretic response of the material up to a pressure of 0.8 MPa is measured using an original experimental set-up that combines hydrostatic pressure loading by nitrogen pressurisation and volume measurement thanks to digital image correlation. In terms of volume change vs. pressure, a detailed analysis of the pressurisation and depressurisation paths shows firstly that the macroscopic critical pressure which is surely emerging from the successive buckling of the microspheres does not depend on their concentration in the composite. Secondly, it is established that the unloading path, even if it does not change its slope steeply, admits an inflection point that defines a second critical pressure, that seems to depend on the volume fraction of the microspheres. In the future, these model-free observations will be useful for developing constitutive models for these composites, and in particular for the strain energy density function dedicated to their spherical response.

Keywords: Elastomer matrix-hollow thermoplastic microspheres composites, Hydrostatic experiments, Compressibility, Pressure-volume hysteresis, Buckling pressure

Highlights

- Novel experimental setup for the hydrostatic pressure-volume change response
- Pressure-volume hysteresis of elastomers filled with thermoplastic microspheres
- Model-free analysis of the response with respect to HTMs volume fraction
- Identification of critical pressures during pressure loading and unloading steps
- Insights for constitutive modeling in marine applications

*Corresponding author

1 Introduction

In a recent review of polymer materials used for sound absorption applications in underwater environments, Fu et al. [1] note that for applications where hydrostatic pressure can be high (the authors mention combat submarines), the mechanical performance of the materials must be studied. Indeed, the acoustic performance of structures is affected by their mechanical state. More recently, Lu et al. [2] provide a literature review of Polymer Matrix Solid Buoyancy Materials (PMSBMs) used for marine applications. The authors present the two-component PMSBMs that combine a polymer matrix with hollow polymer microspheres as a good alternative to conventional syntactic foams containing hollow glass microspheres [3].

Over the past ten years or so, composites made of an elastomer matrix (polyurethane or silicone) filled with hollow thermoplastic microspheres (HTMs) have appeared, particularly for underwater defence applications. To avoid prolonging the discussion, we do not propose an exhaustive bibliography on the subject here, the reader is referred to the excellent introduction of the recent article by Nguyen et al. [4]; only relevant references will be given in the remainder of this introduction. Naturally, the design of structures requires the development of mechanical constitutive equations to predict the mechanical response of these composites. The oldest models attempt to predict the hydrostatic response using analytical homogenisation approaches [5, 6]. More recent works propose more complete models combining spheric and deviatoric contributions in tensorial constitutive models [7, 8, 9, 10, 4]. Once the models have been derived, mechanical tests are required to determine their parameters. The major difficulty lies in the hydrostatic response of these materials. Traditionally, for elastomer-HTMs composites, authors consider uniaxial compression tests [11, 12, 9, 4], and sometimes uniaxial tensile tests [13, 14, 15], to determine the hydrostatic response. As pointed out by Brown [16], purely hydrostatic tests are rare and difficult to implement.

The present paper aims to measure the low-pressure hydrostatic response of elastomer-HTMs composites. To this end, a gas pressurisation set-up with DIC measurement of the volume change is developed and used; this is one of the five classical techniques recently listed by Becker et al. [17] for carrying out hydrostatic tests. The aim of the study is twofold: *(i)* to accurately measure the hysteretic pressure-volume response of materials, and *(ii)* to determine the characteristics of the loading and unloading paths of the hysteresis loop in order to provide data for modelling.

2 Methods

2.1 Materials and samples

Materials are made of a polyurethane elastomer matrix filled with HTMs. Six volume fractions of HTMs are considered: 0, 5, 10, 15, 20, and 25% (nominal data given by the supplier). Knowing the density of the elastomer matrix and that of the thermoplastic polymer making up the HTMs, the actual volume fractions are measured with a gas displacement pycnometer (AccuPyc 1345 from micrometrics). The precision of the volume measurement is ± 0.05 cm^3 and that of the mass measurement is $\pm 10^{-4}$ g. Each sample was measured five times and the corresponding mean values are given in Table 1. These results are in very good agreement with the ones given

Nominal HTMs volume fraction (%)	5	10	15	20	25
Actual HTMs volume fraction ±0.20 (%)	4.69	9.11	13.44	17.68	22.55

Table 1: Nominal and actual volume fractions of HTMs in the five filled materials.

in Coret et al. [15] obtained by weighing the specimens and measuring their geometry. In the following, the actual values will be considered for the computations, but for the sake of simplicity the nominal ones will be used in the presentation of the results.

As shown in Figure 1, the samples are cylinders of 30 mm in diameter and 30 mm thick. They are obtained by water jet cutting in a 30 mm thick sheet.

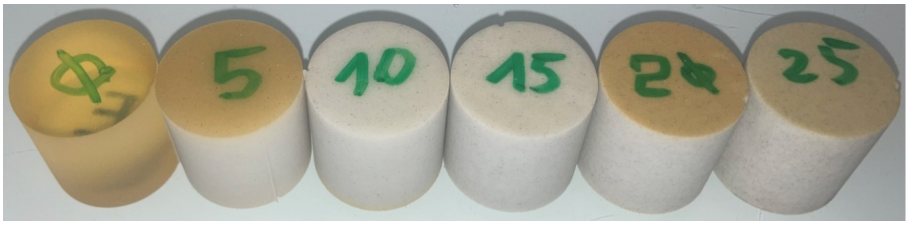

Figure 1: Samples. Numbers stand for the nominal HTMs volume fractions.

2.2 Experimental set-up

The principle of the experiments is simple, as shown in Figure 2. A sample is placed in the

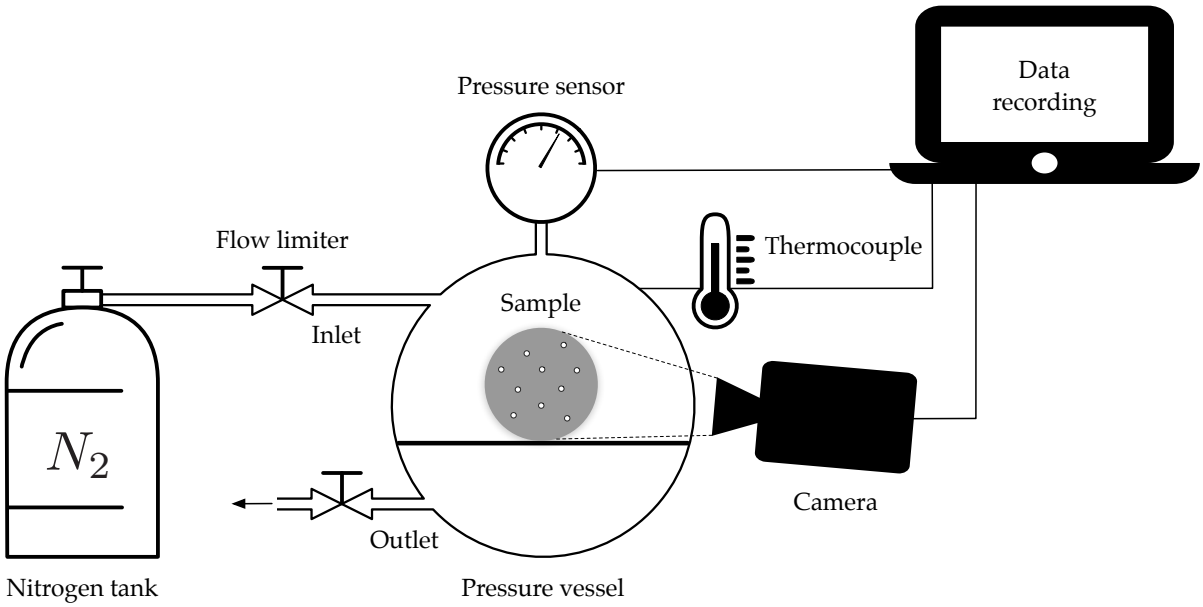

Figure 2: Principle of the experiments.

pressure vessel, a thick metallic closed cylinder, where the pressure is imposed thanks to a flow of nitrogen. Two flow limiters are used: one for the inlet between the nitrogen tank and the vessel, the other for the outlet between the vessel and the outside environment. Pressure and temperature are measured inside the vessel by a strain gage pressure sensor and a T-type thermocouple, respectively. A camera records the deformation of the specimen throughout the

test. The corresponding photos of the setup are presented in Figure 3.

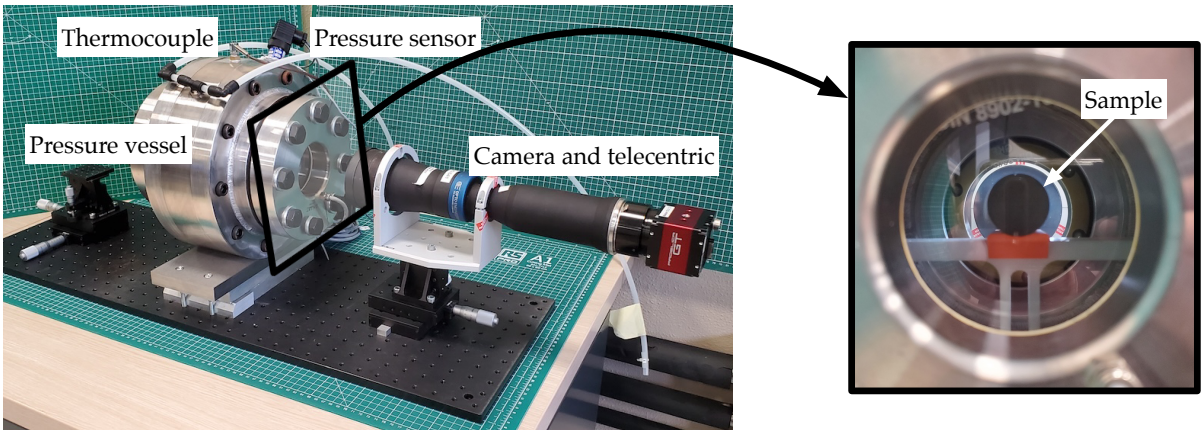

Figure 3: Left: experimental set-up with camera positioning. Right: zoom on the sample placed in the pressure vessel.

Concerning the measuring equipment, the pressure sensor is an Aek BCT-22-10B-V-G1/2-C-S30; it delivers an output voltage ([0, 10 V]) proportional to the pressure in the vessel ([0, 1 MPa]) and the T-type thermocouple is insulated in a 0.5 mm stainless steel sheath connected to a Display-conditioner Trumeter APM-TEMP-ANO. The camera is AVT Prosilica GT 6600 with Opto-Engineering TC16M056 telecentric lens. Lighting is provided by CCS PD2-324 lamps. Pictures are analysed by the digital image correlation (DIC) software Ufreckles [18]. The relevant camera and software parameters are summarized in Table 2.

Camera	29 Megapixel AVT Prosilica GT 6600
Image resolution	6004× 4384 px^2
Lens	Opto Engineering TC16M056 (× 0.641)
Field of view	56 × 37.3 mm^2
Image scale	1 px = 9.33 μm
Patterning technique	Spray paint can
Software	UFreckles
Shape function	Bi-linear quadrilateral Lagrange element (Q4P1)
Element size	[50 50] px^2 / [0.46 0.46] mm^2

Table 2: Parameters of the cameras and the DIC software.

The materials being assumed homogeneous, pictures are analysed by the Gage module of Ufreckles; it calculates the mean principal strains on the circular section of the sample (see Fig. 3-right). Due to hydrostatic loading, every directions in this section of the sample are principal directions of strain. Furthermore, as the materials are isotropic, the out-of-plane strain (which cannot be measured) is also principal and considered to be equal to the in-plane ones. Thus, adopting the small strain assumption and denoting ε_I and ε_{II} the principal strains given by the software, the relative change in volume is

$$\frac{\Delta V}{V} = \frac{3}{2}\left(\varepsilon_I + \varepsilon_{II}\right). \tag{1}$$

Practically, pressure and temperature measurements, and pictures of deformed samples are synchronized at a rate of one per minute.

2.3 Loading conditions

Nitrogen is injected very slowly into the vessel to reach a maximum relative pressure of 0.8 MPa. The nitrogen is then slowly evacuated. The corresponding evolution of pressure and temperature during this cycle is shown in Figure 4. Neither the pressure loading nor the unloading curve is

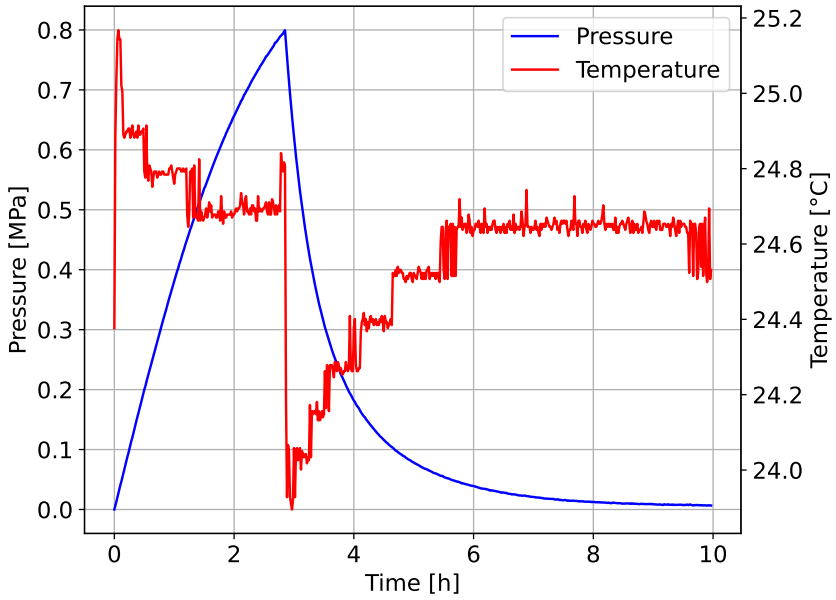

Figure 4: Pressure and temperature loading-unloading cycle.

linear: this is the result of the constant opening of the flow limiters. More precisely, the pressure increases almost linearly from 0 to 0.8 MPa during 3 h and it decreases exponentially from 0.8 to 0 MPa during 7 h. This difference can be explained by the fact that the pressure difference between the nitrogen tank and the pressure vessel (during gas injection) is much greater than that between the vessel and the atmospheric pressure (during emptying). As expected, pressurization and depressurization involve a slight temperature change (less than 1.5°C) inside the vessel.

Each experiment is conducted twice with the same sample.

3 Results and discussion

Given the very slow rate of nitrogen injection and emptying, the mechanical response of the materials is considered to be quasi-static in the following (the order of magnitude of the strain rate is 10^{-6} s^{-1}).

3.1 Change in volume vs. pressure curves

Figure 5 presents the volumetric response, i.e. the change in volume vs. hydrostatic pressure curves, for the five HTMs volume fractions. Firstly, the curves of the five composite materials are similar: they exhibit a hysteresis loop that reflects the different behaviours of the materials

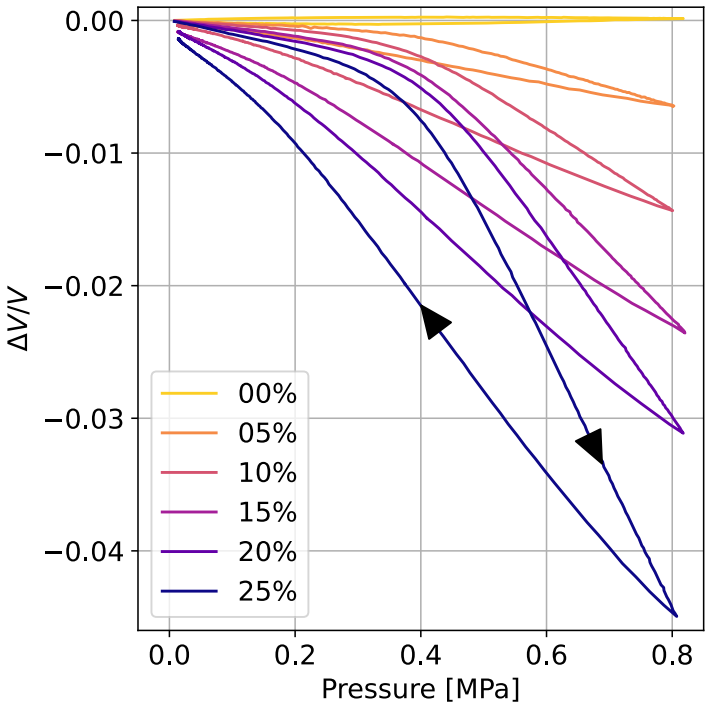

Figure 5: Volumetric response of the five composites under hydrostatic loading conditions.

between loading (increase in pressure) and unloading (decrease in pressure). Secondly, as shown in Figure 6, the size of the hysteresis loop varies considerably according to the volume fraction of microspheres in the material: the more fillers the material contains, the larger the hysteresis loop.

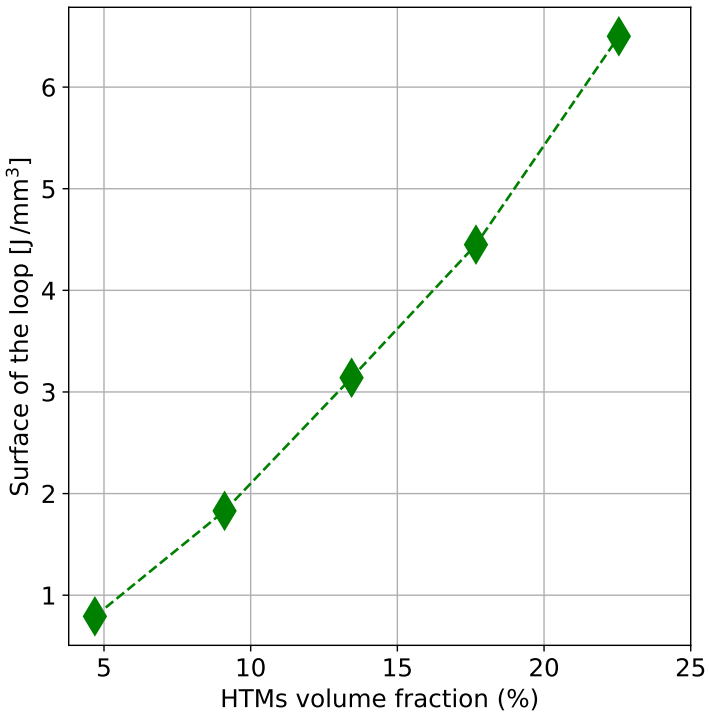

Figure 6: Size of the hysteresis loop vs. volume fraction of microspheres.

This type of response for elastomers with HTMs has already been observed for other types of loading conditions: uniaxial compression [11] and uniaxial tension [15]. The characteristics of the volumetric response described above are directly linked to the microstructural phenomena involved:

- As stated in literature [19, 12], the microspheres buckle one after the other with respect to their radius during the increase in pressure. On a macroscopic scale, it results in a change in slope of the loading curve due to the emergence of a critical pressure. In the following, this pressure is referred to as the "buckling pressure". This behaviour has already been exhibited in uniaxial compression [20] and modeled in hydrostatic compression [6].

- The change in slope of the unloading curve is much less marked, or even seems non-existent for low HTMs volume fractions. The associated microstructural phenomena have not yet been fully elucidated in the literature.

3.2 Quantitative analysis of the hysteresis loop

In order to study the previous curves without invoking a model, the loading and unloading paths of the hysteresis loops will be studied separately. In order to increase the reliability of our results, two different methods are used to extract the trends of the curves.

- The first one is the Ramer-Douglas-Peucker curve simplification method [21, 22], which aims to reduce the number of points on a curve while preserving its overall shape. The simplified points are then used to calculate the slopes of the segments formed between them, which reflect the local changes in the curve. Finally, the change between the successive slopes is calculated to identify the critical pressure: this is defined by the maximum variation in the slope. In this method, the parameter to be supplied by the user is the simplification threshold, which was set here by trial and error.

- The second algorithm is the segmented linear regression analysis. The curve is segmented to minimise the total error, and the slopes of each segment are calculated using a least-square fit. As with the previous method, the change between successive slopes is used to determine the critical pressure. In this method, the parameter to be supplied by the user is the number of segments; here it was determined by trial and error.

In practice, the analysis of the loading and unloading parts of the hysteresis loops is performed in three steps:

(a) the experimental curve is simplified by the algorithm,

(b) the evolution of its slope is calculated,

(c) the relevant values of critical pressure are extracted.

3.2.1 Loading path: buckling pressure

Figure 7 presents the loading curves for the five volume fractions of microspheres.

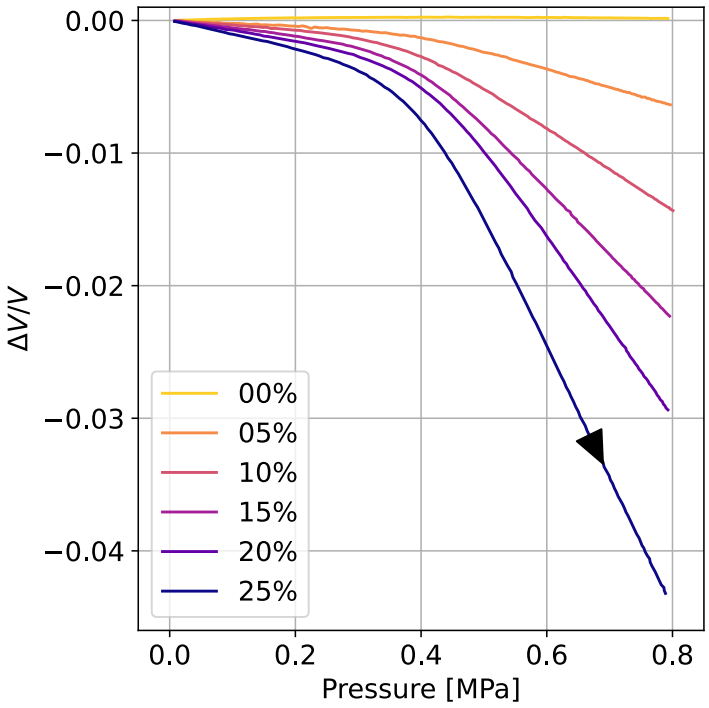

Figure 7: Volumetric response of the five composites for increasing hydrostatic pressure.

The three curves of steps (a), (b), and (c) applied to the loading path have the same shape for all materials regardless of their nominal HTMs volume fraction. In order to illustrate the method, the above-mentioned three steps are presented in Figure 8 for the material with 25% HTMs volume fraction. The corresponding figures for the other HTMs volume fraction are given in appendix A.

The curve of the slope (middle graphs in Fig. 8) is monotonically decreasing and always negative. As a result, the second derivative is also always negative: there is no inflection point in the loading path. Finally, the buckling pressure is defined by the abscissa of the minimum of the second derivative of the simplified curve (bottom graphs in Fig. 8). The corresponding results are presented in Table 3. In practice the simplification threshold varies from 0.7×10^{-4}

Nominal HTMs volume fractions (%)	**5**	**10**	**15**	**20**	**25**
Buckling pressure (MPa) (Ramer-Douglas-Peucker)	0.38	0.40	0.39	0.38	0.40
Buckling pressure (MPa) (segmented linear regression)	0.43	0.40	0.39	0.43	0.42
Buckling pressure (MPa) (mean value)	0.40	0.40	0.39	0.40	0.41

Table 3: Buckling pressures for the loading path of the hydrostatic pressure test.

and 2.0×10^{-4} for the Ramer-Douglas-Peucker method, and the number of segments varies from 5 to 14 for the segmented linear regression technique.

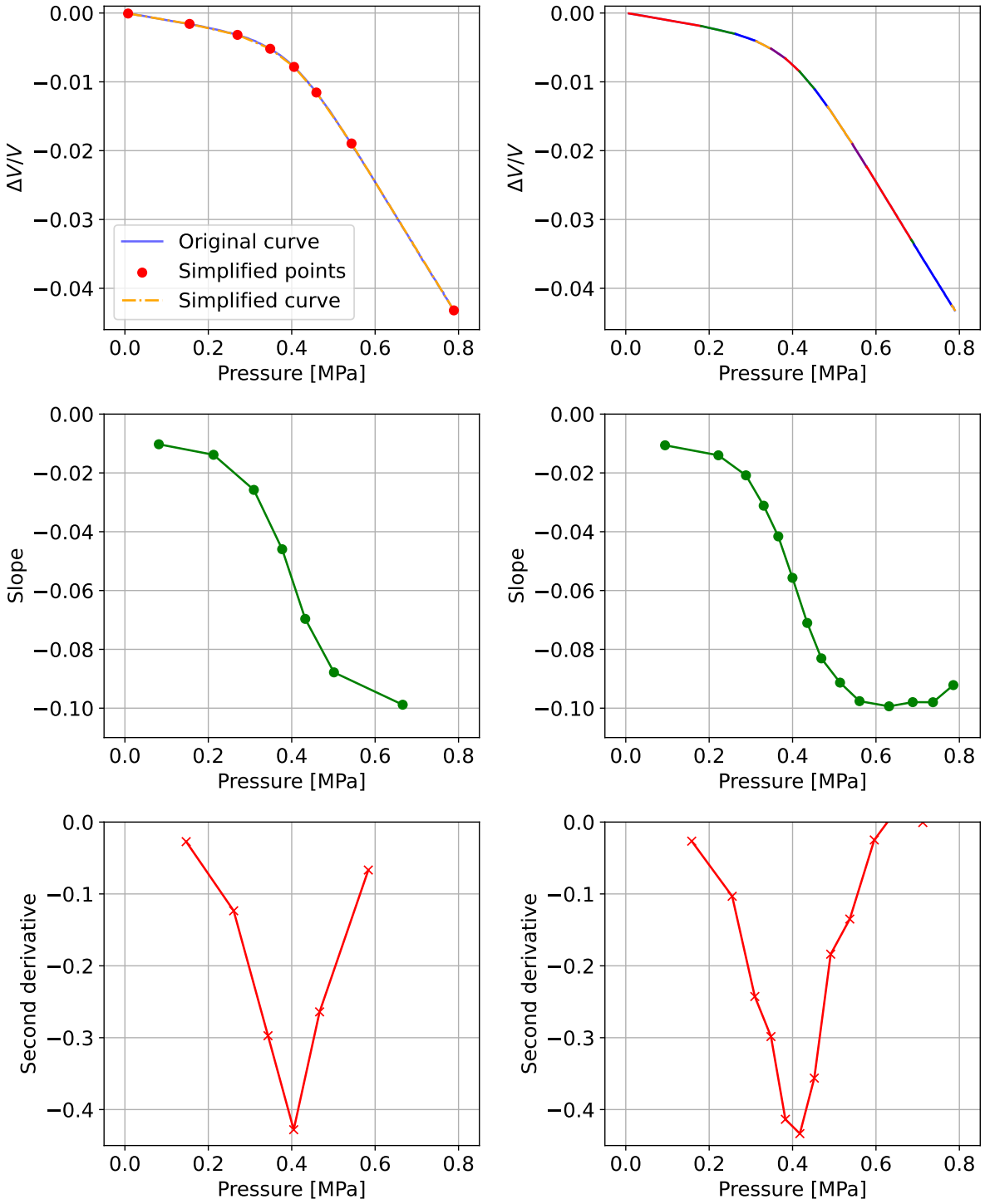

Figure 8: Analysis of the loading path of the 25% filled elastomer. Left: Ramer-Douglas-Peucker method; Right: segmented linear regression. Top: simplified curves (step (a)); Middle: slope of the simplified curve (step (b)); Bottom: second derivative and buckling pressure (step (c)).

3.2.2 Unloading path: inflection pressure

Figure 9 presents the unloading curves for the five volume fractions of microspheres.

All materials admit the same shapes for the three curves of steps (a), (b), and (c). The method applied to the unloading path of the hysteresis loop is illustrated in Figure 10 for the

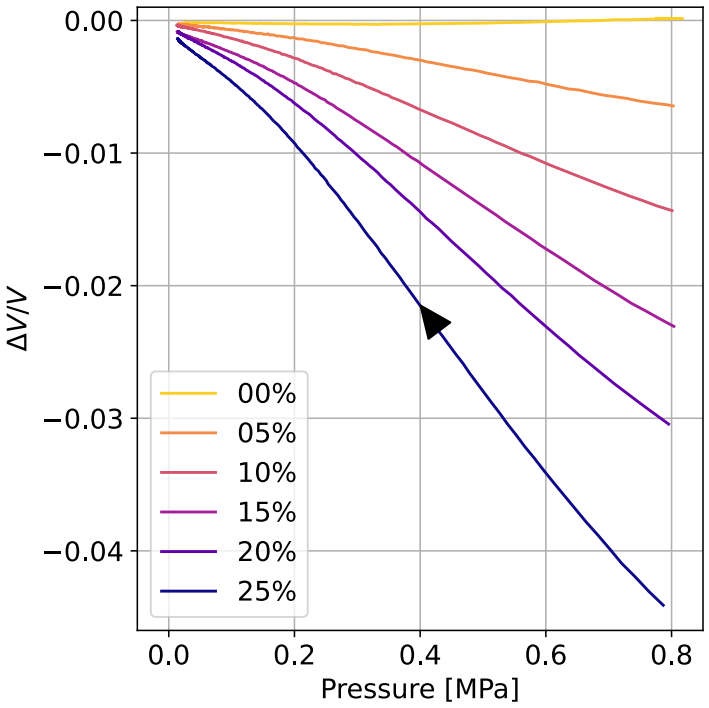

Figure 9: Volumetric response of the five composites for decreasing hydrostatic pressure.

material with 25% of HTMs in volume. The corresponding figures for the other HTMs volume fraction are given in appendix B.

The curve of the slope (middle graphs in Fig. 10) is always negative but is not monotonic. As a result, the second derivative changes sign: the load curve therefore has an inflection point. Finally, we identify this inflection pressure by its corresponding value on the second derivative curve (bottom curves in Fig. 10). The corresponding results are presented in Table 4. In practice

Nominal HTMs volume fraction (%)	**5**	**10**	**15**	**20**	**25**
Inflection pressure (MPa) (Ramer-Douglas-Peucker)	0.49	0.45	0.50	0.45	0.43
Inflection pressure (MPa) (segmented linear regression)	0.45	0.46	0.48	0.46	0.44
Inflection pressure (MPa) (mean value)	0.47	0.46	0.49	0.45	0.44

Table 4: Inflection pressure in the unloading path of the hydrostatic pressure test.

the simplification threshold varies from 0.7×10^{-4} and 1.4×10^{-4} for the Ramer-Douglas-Peucker method. The number of segments varies between 5 and 6 for the segmented linear regression technique; nevertheless due to the shape of the unloading paths, the segmented linear regression technique is difficult to applied.

3.2.3 Summary

The previous results are summarized in Figure 11. Firstly, it should be noted that the material

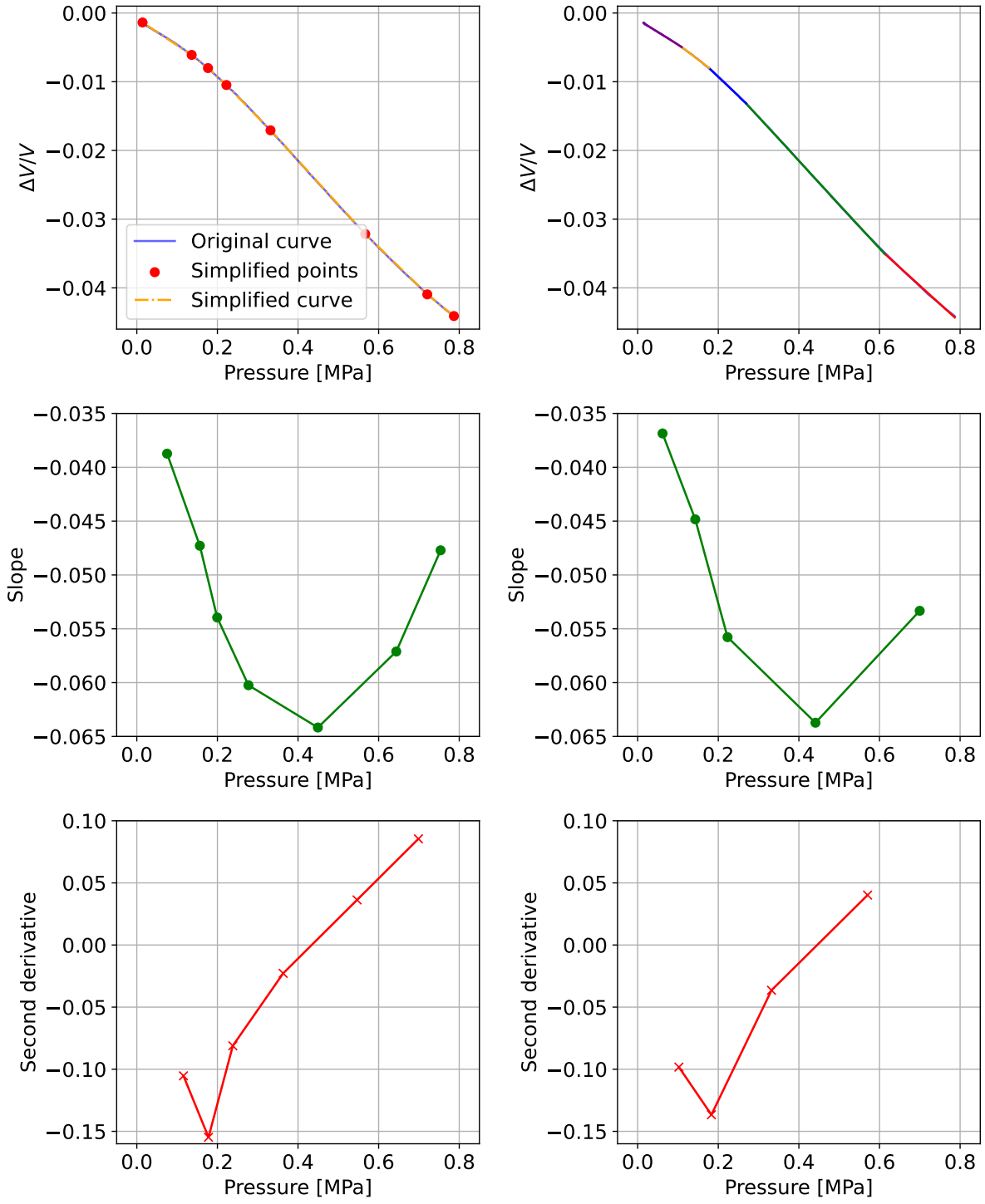

Figure 10: Analysis of the unloading path of the 25% filled elastomer. Left: Ramer-Douglas-Peucker method; Right: segmented linear regression. Top: simplified curves (step (a)); Middle: slope of the simplified curve (step (b)); Bottom: second derivative and inflection pressure (step (c)).

filled with 15% microspheres behaves a little differently to other materials. We have already observed this difference in uniaxial tension [15], which leads us to believe that there may have been a problem in the formulation or manufacture of this material. We will therefore leave it

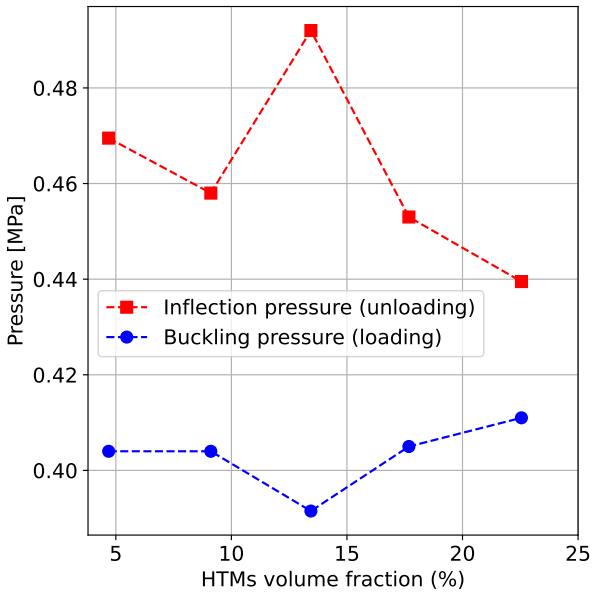

Figure 11: Buckling pressure (loading path) and inflection pressure (unloading path) for the five materials.

aside in the following comments.

On the one hand, the buckling pressure does not seem to depend on the amount of microspheres contained in the composite. This result is in agreement with the predictions of the De Pascalis et al. model [6], which states that this pressure depends only on the distribution of the thickness-radius ratio of the microspheres but not on their concentration in the composite (for volume fractions where there is no interaction between the microspheres). On the other hand, the inflection pressure of the unloading path, which is always higher than the buckling pressure, seems to decrease with the volume fraction of microspheres in the material; this result has never been studied in the literature. Note that for the moment, it is difficult to relate this pressure inflection with microstructural events. To do this, it will be necessary to make microstructural observations in situ, but also to conduct other mechanical tests (cyclic ones, for example).

4 Concluding remarks

This study investigated the hydrostatic response of elastomer-HTMs composites under low pressure loading conditions. The main objectives were to measure the hysteretic pressure-volume change response and to determine the characteristics of the loading and unloading paths of the corresponding hysteresis loop, by not using any model. The experimental set-up, comprising a gas pressurisation system with DIC measurement of the volume change, enabled the hydrostatic response to be captured effectively. The results showed that the size of the hysteresis loop increases with the volume fraction of the microspheres. A model-free analysis of the loading and unloading paths revealed that the buckling pressure during loading is relatively independent of the HTMs volume fraction, which is consistent with previous models. However, the inflection pressure in the unloading path seems to decrease with increasing volume fraction, a phenomenon that has not been studied in depth until now.

References

[1] Y. Fu, I. I. Kabir, G. H. Yeoh, and Z. Peng. A review on polymer-based materials for underwater sound absorption. *Polymer Testing*, 96:107115, 2021.

[2] X. Lu, Y. Li, Z. Chen, S. Li, X. Wang, and Q. Liu. Recent trends in polymer matrix solid buoyancy materials: a review. *Polymers*, 16:2307, 2024.

[3] N. Gupta, S. E. Zeltmann, V. C. Shunmugasamy, and D. Pinisetty. Applications of polymer matrix syntactic foams. *JOM: the Journal of the Minerals, Metals & Materials Society*, 66(2):245–254, 2014.

[4] S.-N. Nguyen, R. De Pascalis, Z. Yousaf, and W. J. Parnell. All-polymer syntactic foams: linking large strain cyclic experiments to quasilinear viscoelastic modelling for materials characterisation. *Composites Part B: Engineering*, 288:111866, 2025.

[5] G. Gaunaurd, E. Callen, and J. Barlow. Pressure effects on the dynamic effective properties of resonating perforated elastomers. *The Journal of the Acoustical Society of America*, 76(1):173–177, 1984.

[6] R. De Pascalis, I. D. Abrahams, and W. J. Parnell. Predicting the pressure–volume curve of an elastic microsphere composite. *Journal of the Mechanics and Physics of Solids*, 61(4):1106–1123, 2013.

[7] B. Shrimali, W. J. Parnell, and O. Lopez-Pamies. A simple explicit model constructed from a homogenization solution for the large-strain mechanical response of elastomeric syntactic foams. *International Journal of Non-Linear Mechanics*, 126:103548, 2020.

[8] K. Ghosh, B. Shrimali, A. Kumar, and O. Lopez-Pamies. The nonlinear viscoelastic response of suspensions of rigid inclusions in rubber: I—Gaussian rubber with constant viscosity. *Journal of the Mechanics and Physics of Solids*, 154:104544, 2021.

[9] M. J. A. Smith, Z. Yousaf, P. Potluri, and W. J. Parnell. Modelling hollow thermoplastic syntactic foams under high-strain compressive loading. *Composites Science and Technology*, 213:108882, 2021.

[10] M. Bour, S. Méo, G. Le Quilliec, F. Chalon, M. Raymond, and D. Picart. Phenomenological constitutive laws for the dissipative behaviour of highly compressible elastomers and their finite element implementation. *European Journal of Mechanics - A/Solids*, 109:105442, 2025.

[11] Z. Yousaf, M. Smith, P. Potluri, and W. Parnell. Compression properties of polymeric syntactic foam composites under cyclic loading. *Composites Part B: Engineering*, 186:107764, 2020.

[12] B. Paget, M. Zinet, and P. Cassagnau. Syntactic foam under compressive stress: comparison of modeling predictions and experimental measurements. *Journal of Cellular Plastics*, 57(3):329–346, 2021.

[13] R. Shorter, A. G. Thomas, J. J. C. Busfield, and J. D. Smith. The physical behaviour of elastomers containing hollow spherical fillers. In A. Boukamel, L. Laiarinandrasana, S. Méo, and E. Verron, editors, *Constitutive Models for Rubber V: Proceedings of the 5th European Conference*, pages 107–112. CRC Press, 2007.

[14] Z. Yousaf, N. F. Morrison, and W. J. Parnell. Tensile properties of all-polymeric syntactic foam composites: experimental characterization and mathematical modelling. *Composites Part B: Engineering*, 231:109556, 2022.

[15] M. Coret, E. Verron, P. Rublon, and B. Leblé. Remarkable response of hollow thermoplastic microspheres-elastomer matrix composites in uniaxial tension. *Mechanics of Soft Materials*, 4(8), 2022.

[16] R. Brown. *Physical Test Methods for Elastomers*. Springer International Publishing AG, 2018.

[17] J. Becker, M. Le Saux, P. Charrier, W. Hervouet, V. Le Saux, L. Maheo, and Y. Marco. The SFIR Test: an innovative hydrostatic compression test to characterize the volumetric behavior of polymeric foams. *Experimental Mechanics*, 64(1):1407–1422, 2024.

[18] J. Réthoré. Ufreckles, 2018.

[19] R. Shorter, J. D. Smith, V. A. Coveney, and J. J. C. Busfield. Axial compression of hollow elastic spheres. *Journal of Mechanics of Materials and Structures*, 5(5):693–705, 2010.

[20] L. Tanné, M. Coret, E. Verron, and P. Rublon. Compressive volumetric response of hollow thermoplastic microspheres-elastomer matrix composites. In C. Marano, F. Briatico-Vangosa, L. Andena, and R. Frassine, editors, *Constitutive Models for Rubber XII: Proceedings of the 12th European Conference*, pages 517–522. CRC Press, 2022.

[21] U. Ramer. An iterative procedure for the polygonal approximation of plane curves. *Computer Graphics and Image Processing*, 1(3):244–256, 1972.

[22] D. H. Douglas and T. K. Peucker. Algorithms for the reduction of the number of points required to represent a digitized line or its caricature. *Cartographica*, 10(2):112–122, 1973.

Author contributions: CRedIT

- Ruelle B.: Formal analysis, Investigation, Writing - original draft
- Rublon P.: Conceptualization, Funding acquisition, Project administration, Supervision, Writing - review and editing
- Coret M.: Conceptualization, Data curation, Methodology, Resources, Supervision, Writing - review and editing
- Verron E.: Formal analysis, Visualization, Writing - original draft, Writing - review and editing

Declarations

Conflict of interest: The author declares that he has no conflict of interest

A Loading paths

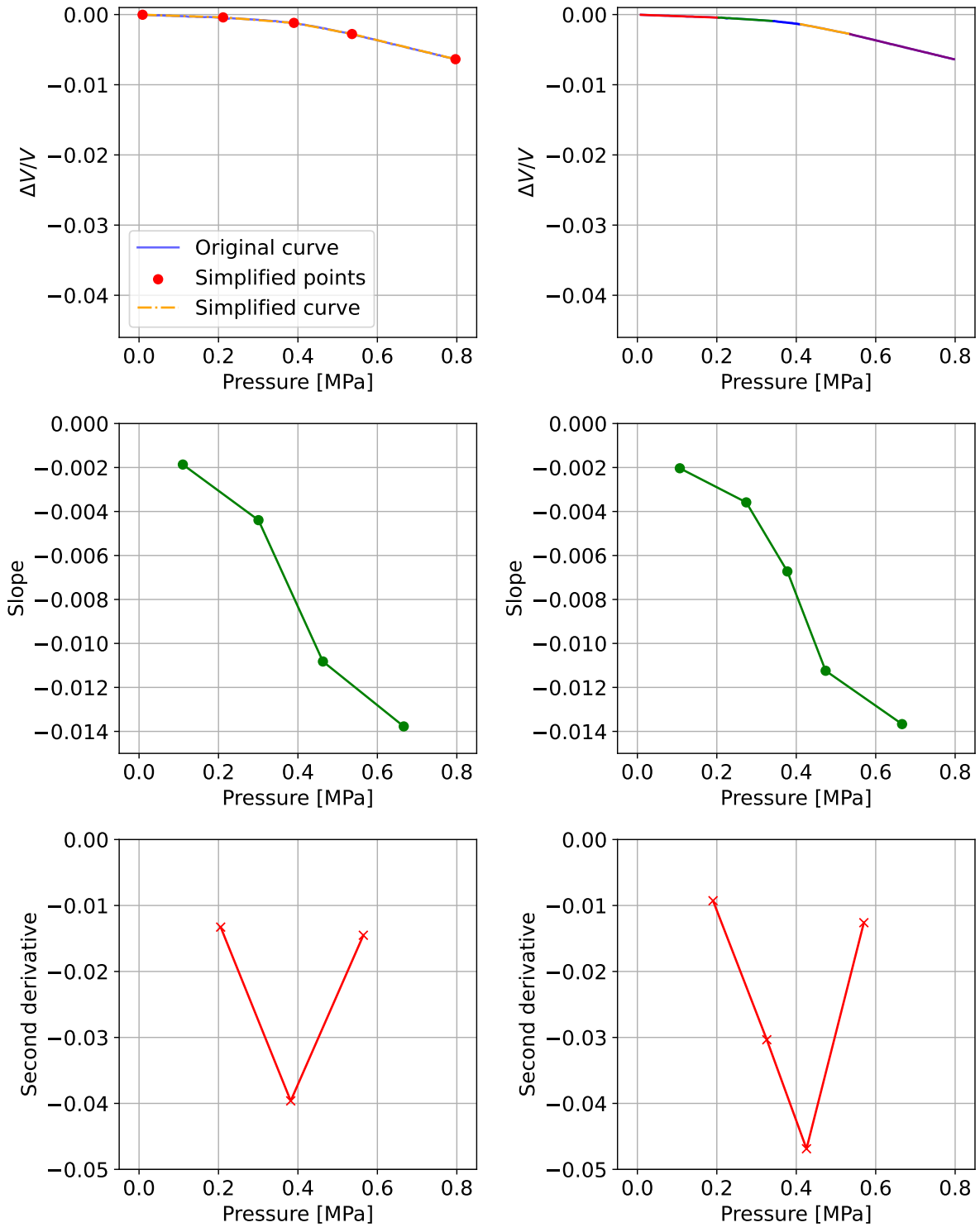

Figure 12: Analysis of the loading path of the 5% filled elastomer. Left: Ramer-Douglas-Peucker method; Right: segmented linear regression. Top: simplified curves (step (a)); Middle: slope of the simplified curve (step (b)); Bottom: second derivative and buckling pressure (step (c)).

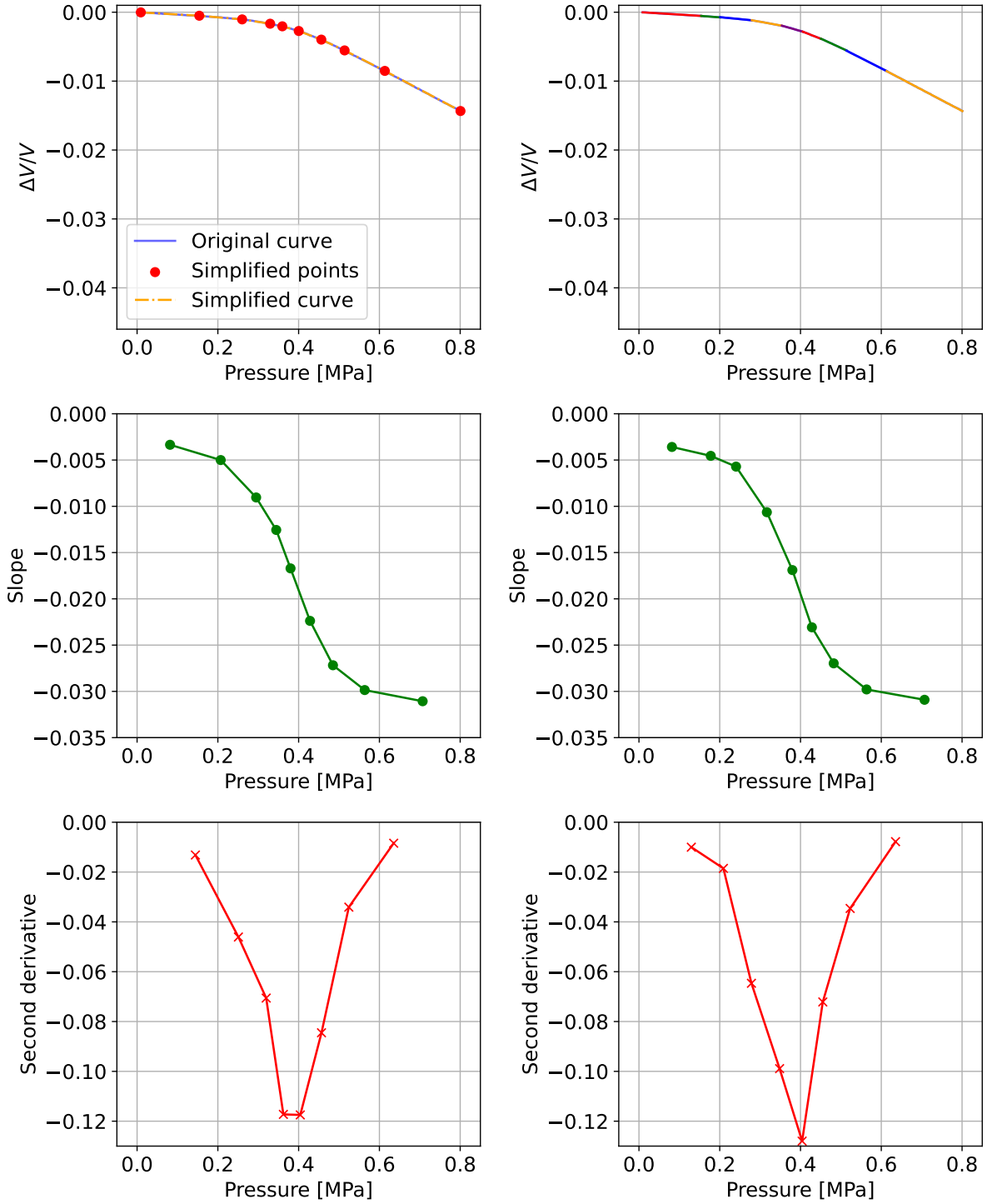

Figure 13: Analysis of the loading path of the 10% filled elastomer. Left: Ramer-Douglas-Peucker method; Right: segmented linear regression. Top: simplified curves (step (a)); Middle: slope of the simplified curve (step (b)); Bottom: second derivative and buckling pressure (step (c)).

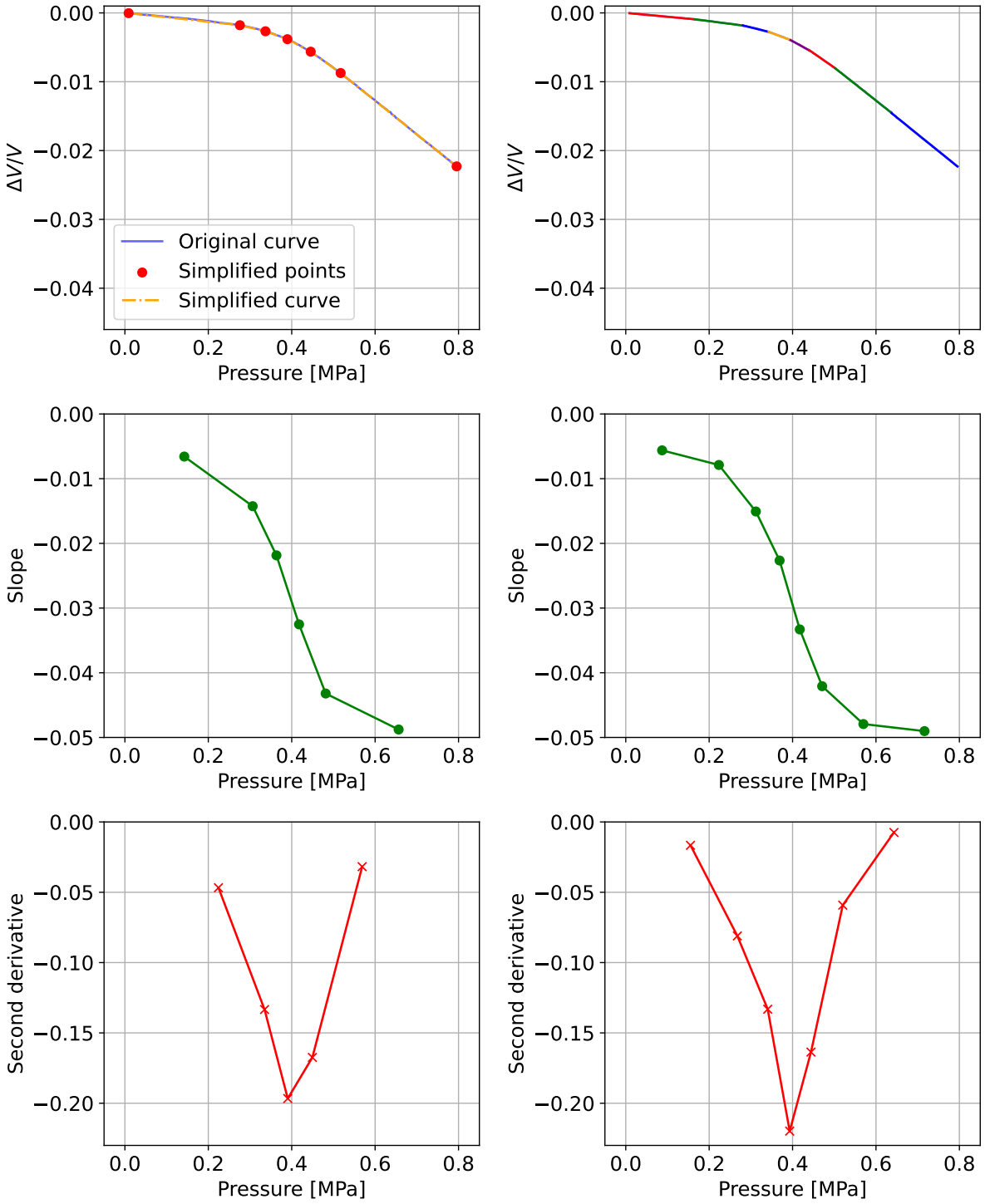

Figure 14: Analysis of the loading path of the 15% filled elastomer. Left: Ramer-Douglas-Peucker method; Right: segmented linear regression. Top: simplified curves (step (a)); Middle: slope of the simplified curve (step (b)); Bottom: second derivative and buckling pressure (step (c)).

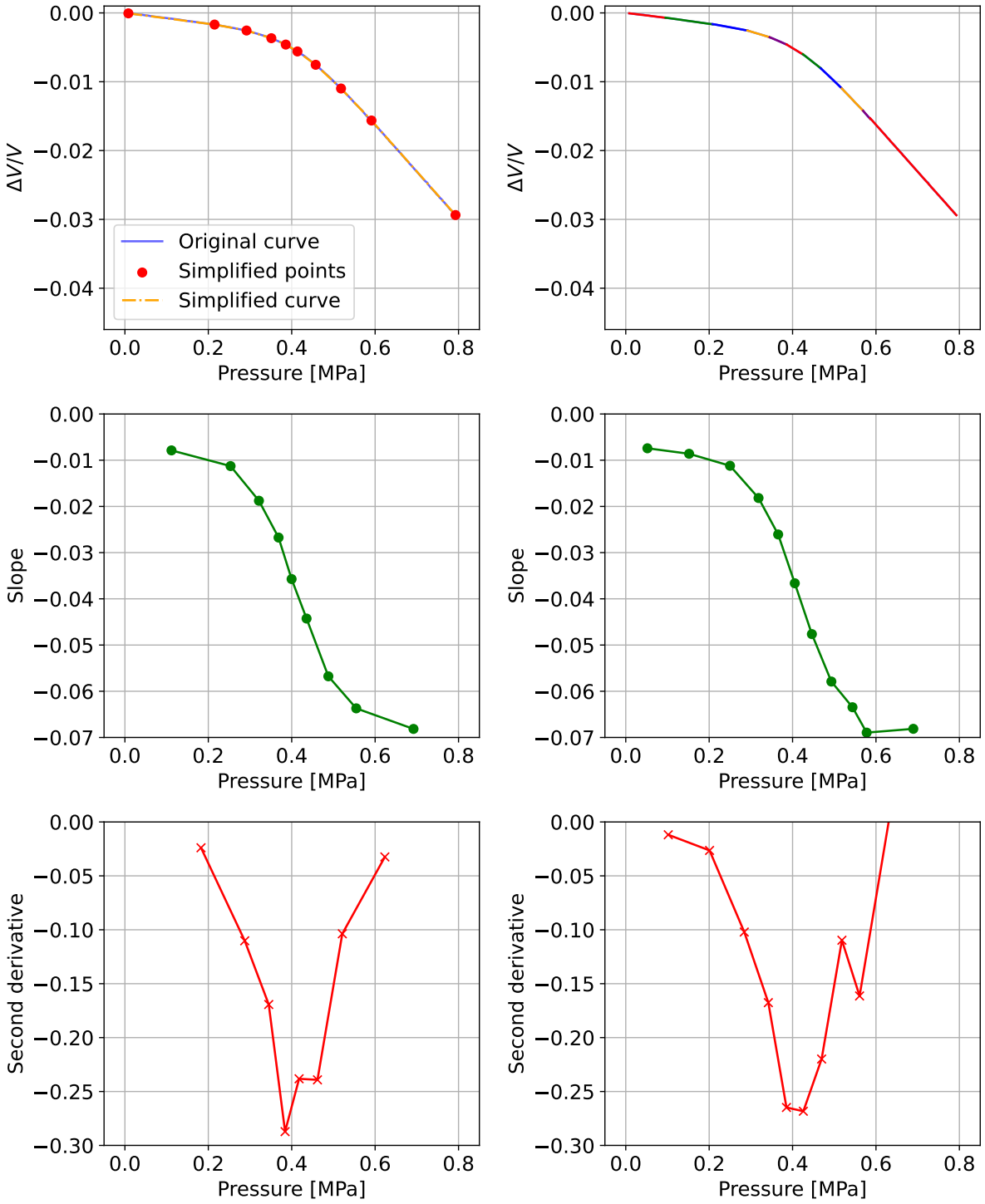

Figure 15: Analysis of the loading path of the 20% filled elastomer. Left: Ramer-Douglas-Peucker method; Right: segmented linear regression. Top: simplified curves (step (a)); Middle: slope of the simplified curve (step (b)); Bottom: second derivative and buckling pressure (step (c)).

B Unloading paths

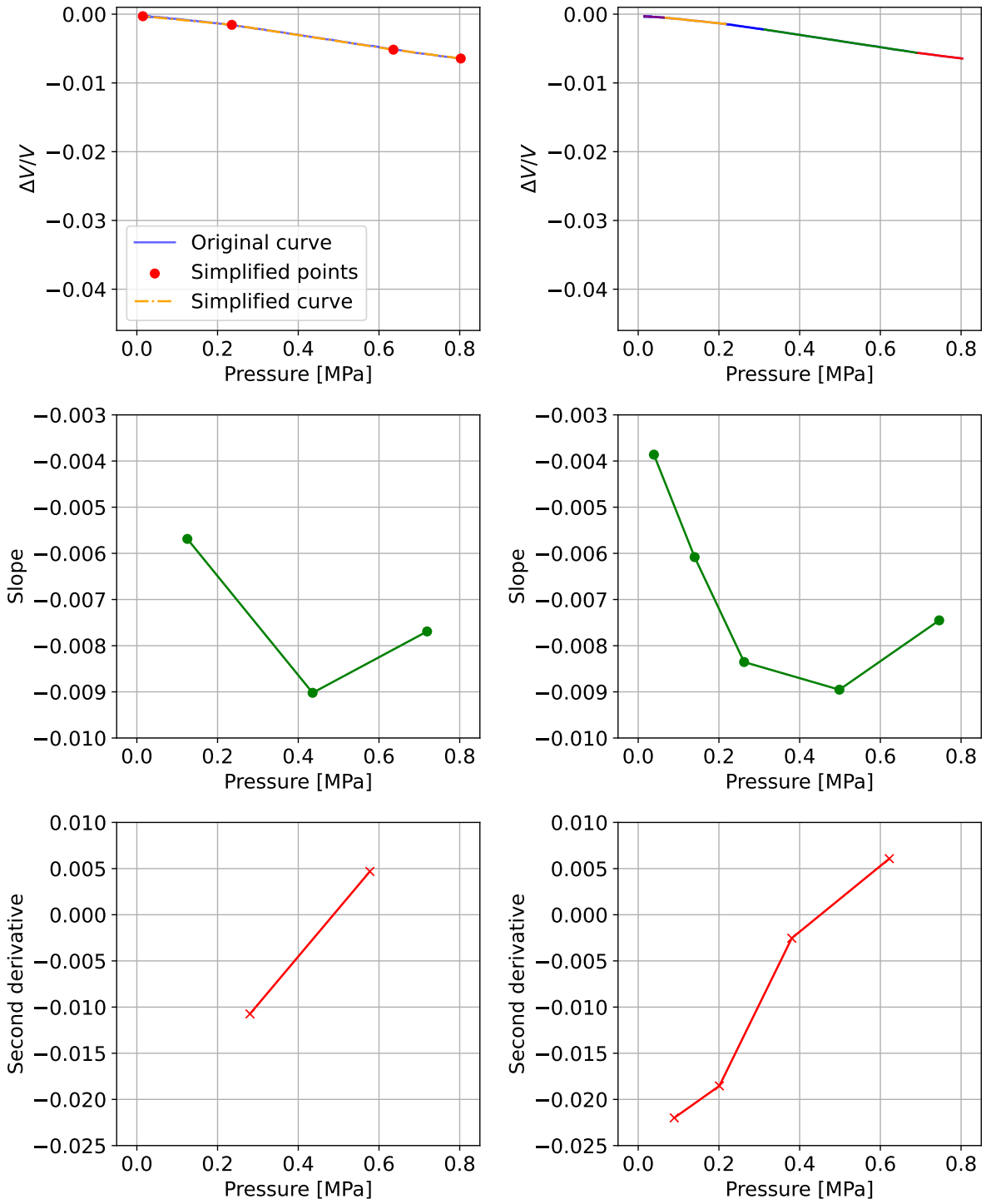

Figure 16: Analysis of the unloading path of the 5% filled elastomer. Left: Ramer-Douglas-Peucker method; Right: segmented linear regression. Top: simplified curves (step (a)); Middle: slope of the simplified curve (step (b)); Bottom: second derivative and inflection pressure (step (c)).

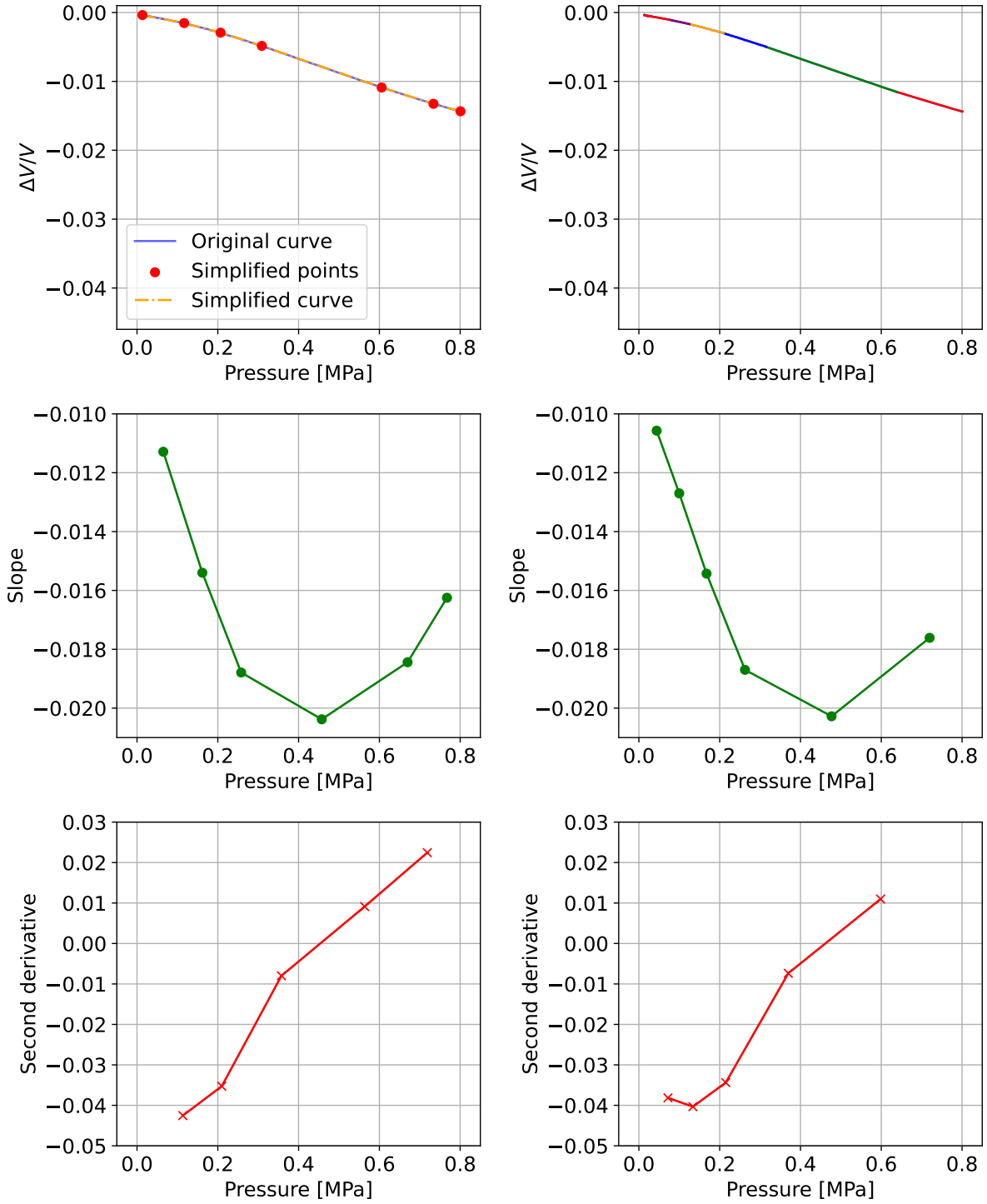

Figure 17: Analysis of the unloading path of the 10% filled elastomer. Left: Ramer-Douglas-Peucker method; Right: segmented linear regression. Top: simplified curves (step (a)); Middle: slope of the simplified curve (step (b)); Bottom: second derivative and inflection pressure (step (c)).

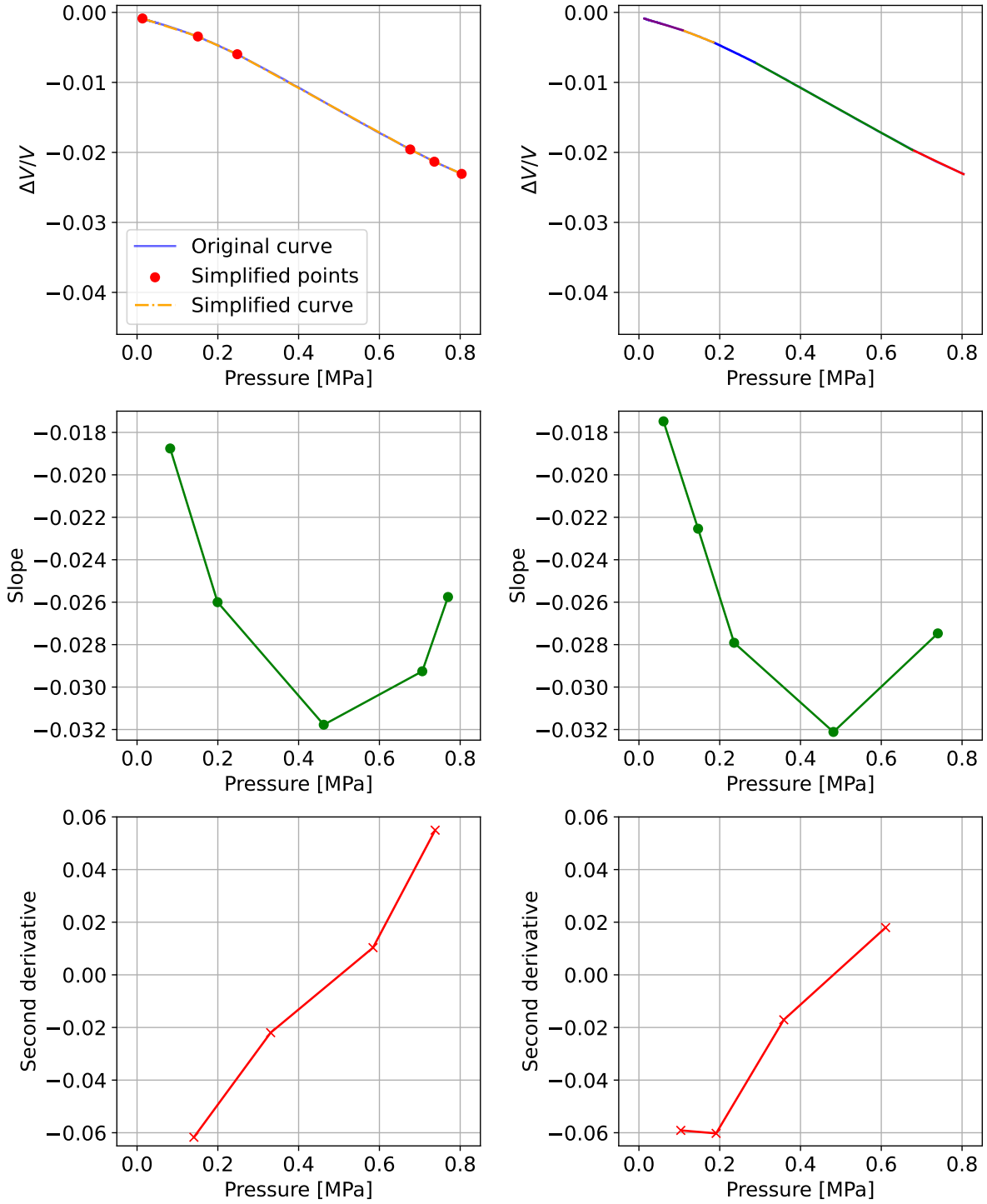

Figure 18: Analysis of the unloading path of the 15% filled elastomer. Left: Ramer-Douglas-Peucker method; Right: segmented linear regression. Top: simplified curves (step (a)); Middle: slope of the simplified curve (step (b)); Bottom: second derivative and inflection pressure (step (c)).

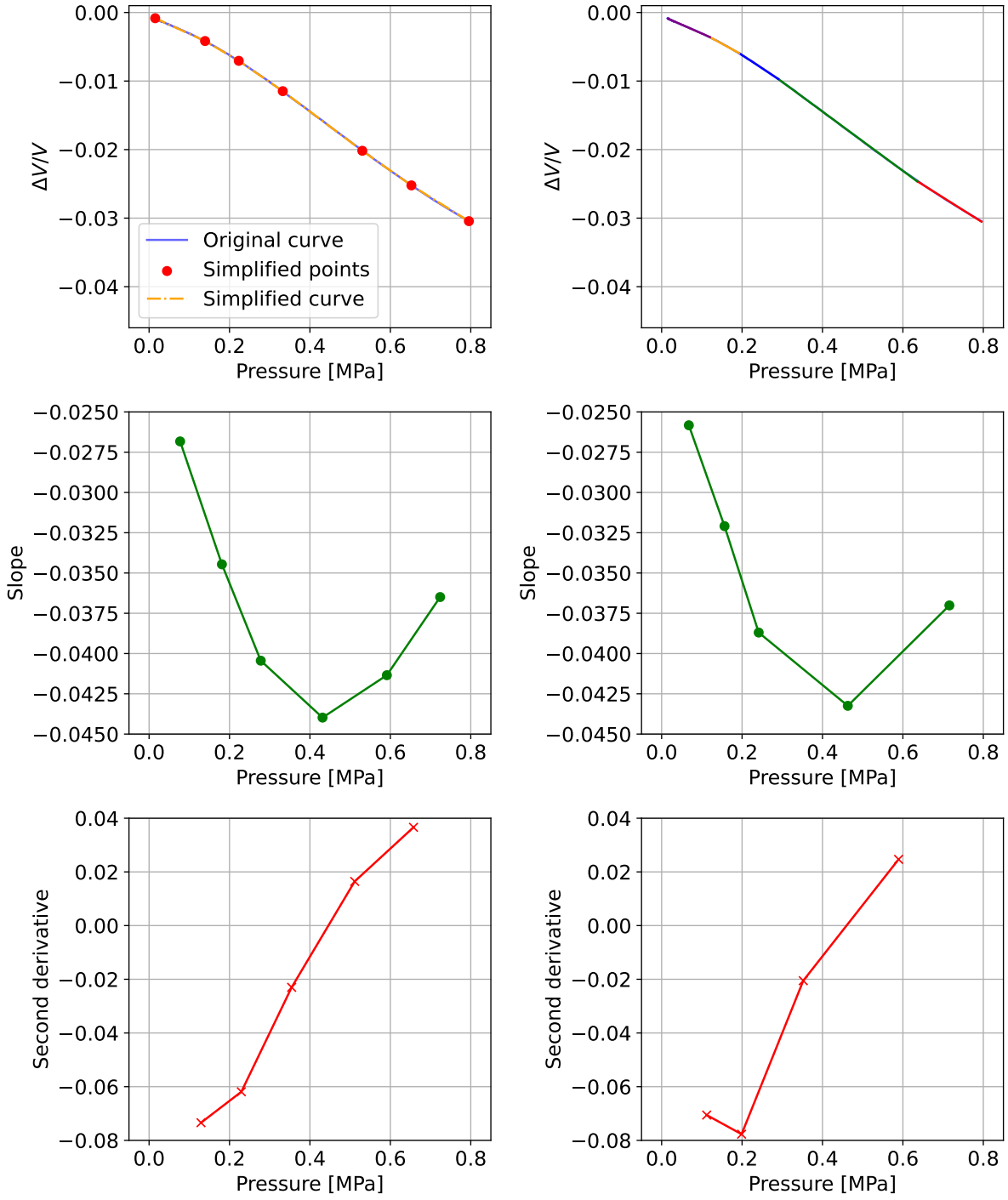

Figure 19: Analysis of the unloading path of the 20% filled elastomer. Left: Ramer-Douglas-Peucker method; Right: segmented linear regression. Top: simplified curves (step (a)); Middle: slope of the simplified curve (step (b)); Bottom: second derivative and inflection pressure (step (c)).